Journal of ELECTRONIC MATERIALS, Vol. 41, No. 4, 2012
DOI: 10.1007/s11664-012-1900-5

Structural, Optical, and Electrical Properties of Cobalt-Doped CdS Quantum Dots

M. THAMBIDURAI,[1,4] N. MUTHUKUMARASAMY,[1] DHAYALAN VELAUTHAPILLAI,[2] S. AGILAN,[1] and R. BALASUNDARAPRABHU[3]

1.—Department of Physics, Coimbatore Institute of Technology, Coimbatore, India. 2.—Department of Engineering, University College of Bergen, Bergen, Norway. 3.—Department of Physics, PSG College of Technology, Coimbatore, India. 4.—e-mail: phy_thambi@rediffmail.com

In the present work, a systematic study has been carried out to understand the influence of cobalt (Co) doping on various properties of CdS nanoparticles. CdS and Co-doped CdS quantum dots have been prepared at room temperature using a chemical precipitation method without using catalysts, capping agents, or surfactants. X-ray diffraction reveals that both undoped and Co-doped CdS nanoparticles exhibit hexagonal structure without any impurity phase, and the lattice constants of CdS nanoparticles are observed to decrease slightly with increasing cobalt concentration. High-resolution transmission electron microscopy (HRTEM) shows that the particle size of CdS and 5.02% Co-doped CdS nanoparticles is in the range of 2 nm to 4 nm. The Raman spectra of Co-doped CdS nanoparticles exhibit a red-shift compared with that of bulk CdS, which may be attributed to optical phonon confinement. The optical absorption spectra of Co-doped CdS nanoparticles also exhibit a red-shift with respect to that of CdS nanoparticles. The electrical conductivity of CdS and Co-doped CdS nanoparticles is found to increase with increasing temperature and cobalt concentration.

Key words: Chemical synthesis, Co-doped CdS, quantum confinement, electrical properties

INTRODUCTION

Quantum dots of II-VI semiconductors have, in particular, attracted attention in recent years because of their easy synthesis in the size range that leads to quantum confinement effects and their potential applications in optoelectronic devices, solar cells, photocatalysis, and sensitized solar cells.[1–3] CdS is an important group II-VI compound semiconductor with excellent physical properties and wide band gap energy of 2.42 eV. CdS can be prepared in one-dimensional nanostructures such as nanowires, nanobelts, and nanorods.[4–6] CdS quantum dots with large optical band gaps are water soluble, biocompatible, and useful as fluorescent biological labels.[7] The Bohr radius of the exciton of CdS is 3 nm, and quantum confinement occurs when the size of the crystallite is around 2 nm to 6 nm and below.[8] This confinement induces discrete electronic states in the valance and conduction band rather than continuous electronic states as in the bulk material.

Introduction of transition metals into nonmagnetic semiconductors provides a possible route for generation of dilute magnetic semiconductors (DMS). CdS-based dilute magnetic semiconductors are good candidates for applications in the areas of magnetic field sensors, spintronics, isolators, magnetic recording, magnetooptical switches, field-emission displays, and gas sensors. Thus, study of the properties of CdS doped with transition metals such as manganese, iron, and cobalt is interesting. CdS nanoparticles after doping with Mn^{2+} and Fe^{2+} exhibited an optical absorption edge shifted towards longer wavelength.[9,10] Zielinski et al.[11] and Seong et al.[12] reported that sp–d exchange interactions in

(Received March 30, 2011; accepted January 2, 2012; published online February 11, 2012)

Co^{2+}-doped II–VI semiconductors are much larger than those in Mn^{2+}-doped counterparts. The Cd ion in the crystal lattice of CdS is surrounded by four S ions forming a tetrahedron. The Co impurity (Co^{2+} ion) replaces the Cd^{2+} ions and considerably influences the optical properties of CdS, enhancing the emission of visible light. To date, very limited work has been carried out on Co-doped CdS nanoparticles, thus making it imperative to understand the influence of Co doping on various properties of CdS nanoparticles. Therefore, in the present work, a systematic study has been carried out on the structural, optical, and electrical properties of undoped CdS and Co-doped CdS nanoparticles.

EXPERIMENTAL PROCEDURES

In the present study, CdS and Co-doped CdS quantum dots were synthesized by a chemical precipitation technique. Aqueous solution of cadmium nitrate [$Cd(NO_3)_2{\cdot}4H_2O$] and the required amount of cobalt(II) nitrate hexahydrate [$Co(NO_3)_2{\cdot}6H_2O$] were mixed thoroughly and stirred for 1 h at room temperature. Aqueous solution of sodium sulfide (Na_2S) was added dropwise to the cadmium nitrate and cobalt nitrate mixture, and the solution was stirred for 2 h. A yellowish-green precipitate was formed soon after the addition of Na_2S. The nanoparticles were initially purified by precipitating the particles with excess double-distilled water. The obtained solution was centrifuged at 4000 rpm for 10 min, then the sample was dried at 100°C for 3 h.

X-ray diffraction studies were carried out using a PANalytical x-ray diffractometer. The surface morphology of the samples was studied using a JEM JEOL-6500 field-emission scanning electron microscope (FESEM). The presence of the elements Cd, S, and Co was identified using energy-dispersive x-ray analysis (EDAX, Thermo-Noran system Six), and high-resolution transmission electron microscopy (HRTEM) images of the prepared CdS and Co-doped CdS samples were recorded using a Philips TECNAI F20 microscope. Raman spectra of the samples were recorded using a Horiba Jobin Yuon HR (800) spectrometer. The optical properties were studied using absorbance spectra recorded by spectrophotometer (JASCO V-570). Electrical measurements were carried out using a Hewlett Packard Precision LCR meter (model 4284A).

RESULTS AND DISCUSSION

The x-ray diffraction patterns of CdS and Co-doped CdS quantum dots are shown in Fig. 1. The diffraction peaks at 2θ values 26.62, 43.97°, and 51.91° are indexed as (002), (110), and (112) planes, corresponding to hexagonal CdS. The lattice constant values were calculated to be a = 4.112 Å and c = 6.690 Å, and are in agreement with the standard data of JCPDS card no. 02-0549. The peaks in the diffraction pattern of Co-doped CdS show a clear shift towards higher 2θ value with increase in cobalt concentration. This shift may be due to occupation of cobalt ions at Cd sites. The structural parameters calculated using the x-ray diffraction pattern are given in Table I. The lattice constants of Co-doped CdS were observed to be slightly smaller than those of CdS, because the ionic radius of Co (0.745 Å) is smaller than that of Cd (0.96 Å). The lattice parameters were found to decrease with increase in cobalt concentration. The average crystallite size was calculated using Scherrer's formula[13]

$$D = \frac{K\lambda}{\beta \cos\theta}, \tag{1}$$

where D is the grain size, K is a constant taken to be 0.94, λ is the wavelength of the x-ray radiation, β is the full-width at half-maximum, and θ is the angle of diffraction. The particle size of CdS and Co-doped CdS nanoparticles was found to lie in the range of 2.9 nm to 4.5 nm (±0.1 nm).

The surface morphology of CdS and Co-doped CdS samples was studied using field-emission scanning electron microscopy (FESEM). FESEM images of CdS and Co-doped CdS nanoparticles are shown in

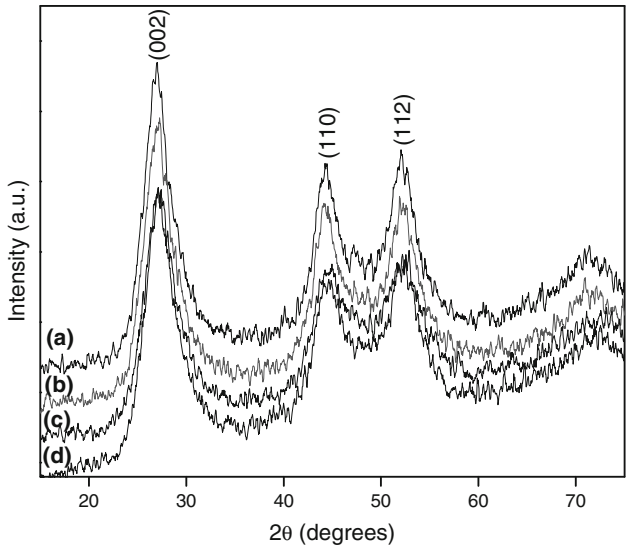

Fig. 1. X-ray diffraction pattern of (a) CdS, (b) 1.20% Co-doped CdS, (c) 5.02% Co-doped CdS, and (d) 7.25% Co-doped CdS nanoparticles.

Table I. Structural parameters of CdS and Co-doped CdS nanoparticles

Material	$2\theta_{(002)}$	d (Å)	Calculated Values		Grain Size (nm)
			a (Å)	c (Å)	
CdS	26.62	3.345	4.112	6.690	2.9
1.20% Co	26.75	3.328	4.100	6.656	3.3
5.02% Co	26.85	3.316	4.094	6.632	3.8
7.25% Co	26.98	3.301	4.086	6.602	4.5

Fig. 2, where it is observed that the particles are very small in size and nearly spherical in shape. Figure 3a–d shows the energy-dispersive x-ray analysis (EDAX) spectra of the CdS and Co-doped CdS, confirming the stoichiometric composition of the CdS and Co-doped CdS samples.

HRTEM images of CdS and 5.02% Co-doped CdS are shown in Fig. 4. It can been seen from Fig. 4b and d that the images have lattice fringes, from which the interplanar spacing can be calculated. The interplanar spacing calculated using the lattice fringes was found to be 3.34 Å and 3.28 Å for CdS and 5.02% Co-doped CdS, respectively, corresponding to the (002) plane of hexagonal CdS. The *d*-spacing values calculated from these images are in close agreement with the values obtained from x-ray diffraction studies. The particle size of the CdS nanoparticles was found to be about ~2 nm. The insets to Fig. 4b, d show selected-area diffraction (SAED) patterns for CdS and 5.02% Co-doped CdS. The selected-area diffraction patterns exhibit concentric circles, revealing that the undoped CdS and Co-doped CdS are nanocrystalline, being made up of small particles. The rings correspond to the (002), (110), and (112) planes of the hexagonal phase. The lattice spacing of 5.02% Co-doped CdS nanoparticles is 3.28 Å, slightly less than that of undoped CdS (3.34 Å) because of the smaller ionic radius of cobalt compared with that of Cd^{2+} (r^{2+}_{Co} = 0.745 Å, r^{2+}_{Cd} = 0.96 Å). The average particle size of the 5.02% Co-doped CdS nanoparticles determined using the HRTEM image is ~4 nm.

Raman spectra of CdS and Co-doped CdS nanoparticles are shown in Fig. 5. Raman peaks are observed at 300 cm^{-1}, 600 cm^{-1}, and 900 cm^{-1}, corresponding to 1LO, 2LO, and 3LO optical phonons of CdS, respectively. These Raman peaks of CdS are in agreement with reported values.[14] From Fig. 5 it is observed that the Raman modes of Co-doped CdS nanoparticles are shifted slightly towards lower wavenumber, being observed at 298 cm^{-1}, 597 cm^{-1}, and 897 cm^{-1}, respectively.

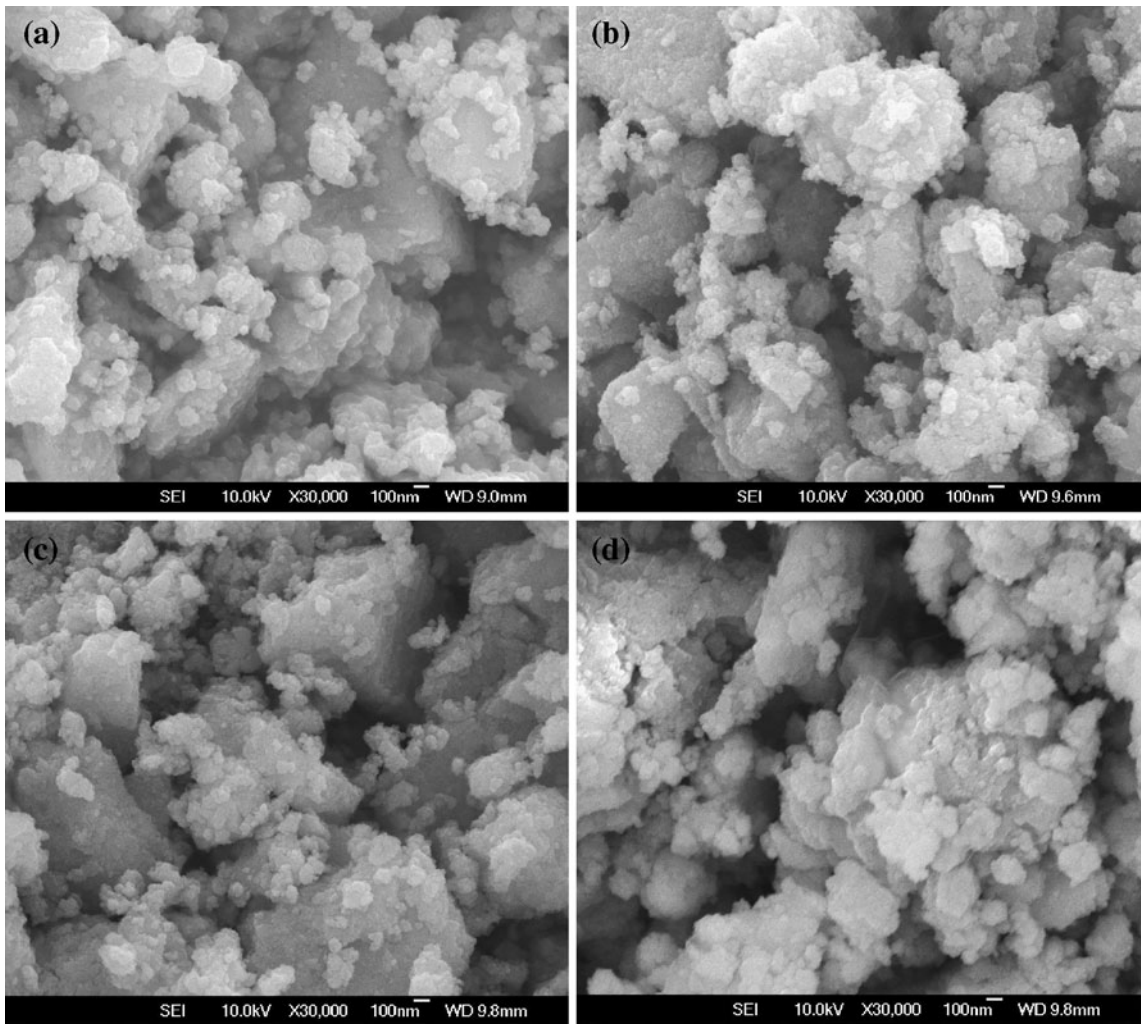

Fig. 2. FESEM images of (a) CdS, and CdS doped with (b) 1.20% Co, (c) 5.02% Co, and (d) 7.25% Co.

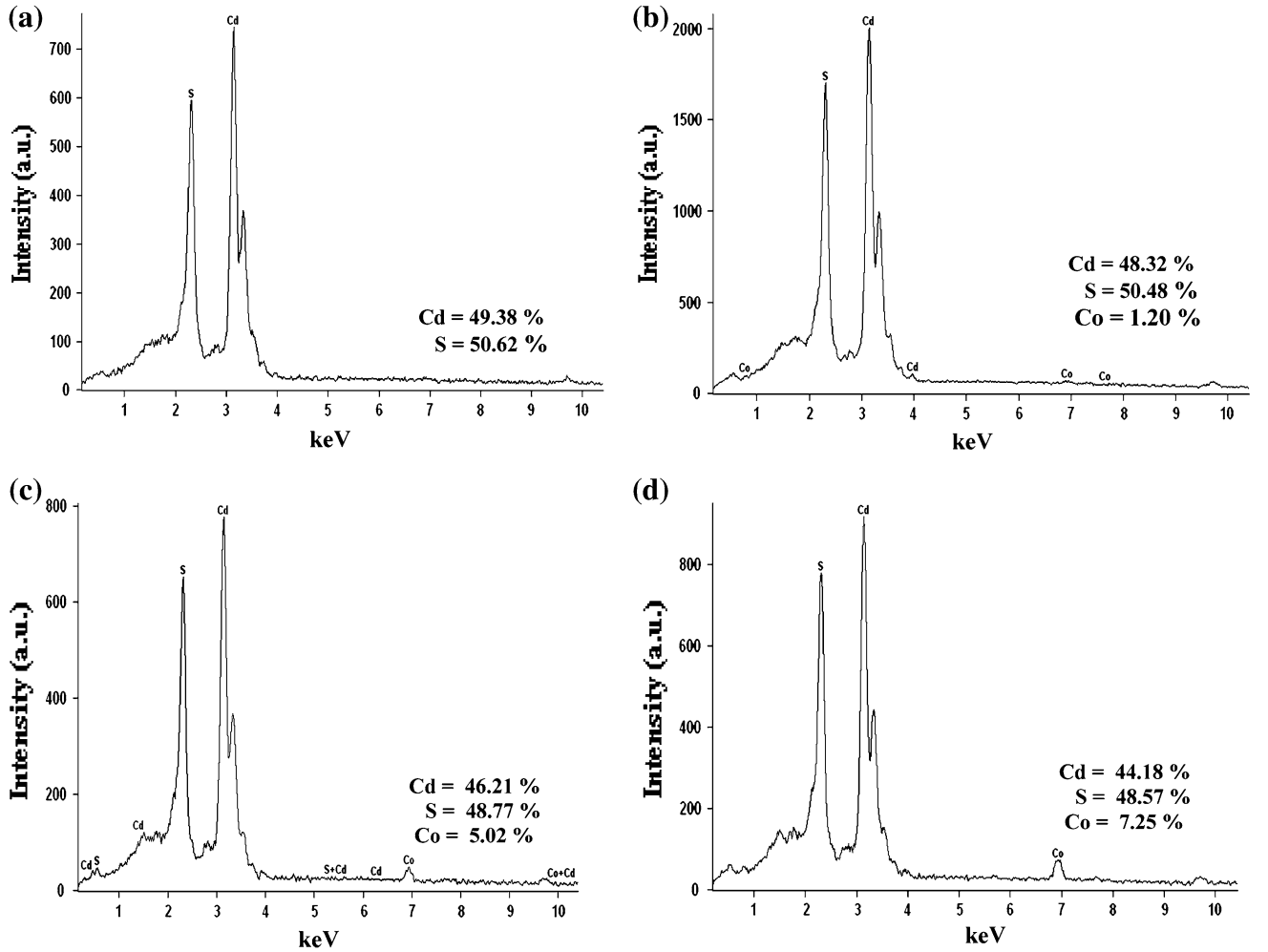

Fig. 3. EDAX pattern of CdS and Co-doped CdS nanoparticles.

Optical absorption spectra of CdS and Co-doped CdS quantum dots are shown in Fig. 6. From the absorption spectra, it is seen that the absorption edge of CdS nanoparticles is blue-shifted, being located at 330 nm, when compared with that of bulk CdS, which has an absorption edge at 512 nm. This blue-shift is mainly attributed to a strong quantum confinement effect caused by the reduction in particle size.[15] It is well known that, in the case of semiconductors, the band gap between the valence and conduction band increases as the size of the particle decreases in the nanosize range. Absorption spectra of Co-doped CdS nanoparticles show that the absorption edge is shifted slightly towards longer wavelength when compared with that of undoped CdS nanoparticles, and this shift is found to increase with increase in cobalt concentration. This shift towards longer wavelength indicates a decrease of the optical band gap.

The fundamental absorption, which corresponds to electron excitation from the valance band to the conduction band, can be used to determine the nature and value of the optical band gap. The relation between the absorption coefficient (α) and the incident photon energy ($h\upsilon$) can be written as

$$(\alpha h\upsilon) = A(h\upsilon - E_g)^n, \tag{2}$$

where A is a constant, E_g is the band gap of the material, υ is the frequency of the incident radiation, h is Planck's constant, and the exponent n is 0.5 for direct allowed transitions. The optical band gap of the CdS and Co-doped CdS nanoparticles was determined using Eq. 2. Figure 7 shows $(\alpha h\upsilon)^2$ versus $h\upsilon$ plot for the CdS and Co-doped CdS nanoparticles. The straight line nature of the plot suggests that the nature of the band gap is direct allowed. The band gap values were determined by extrapolating the linear portion of the curve to meet the $h\upsilon$ axis. The band gap of undoped CdS was obtained as 3.97 eV, and the band gap of 1.20% Co-, 5.02% Co-, and 7.25% Co-doped CdS was found to be 3.91 eV, 3.85 eV, and 3.80 eV, respectively. The band gap is observed to decrease with increase in cobalt concentration. Chandramohan et al.[16] reported that increasing the cobalt

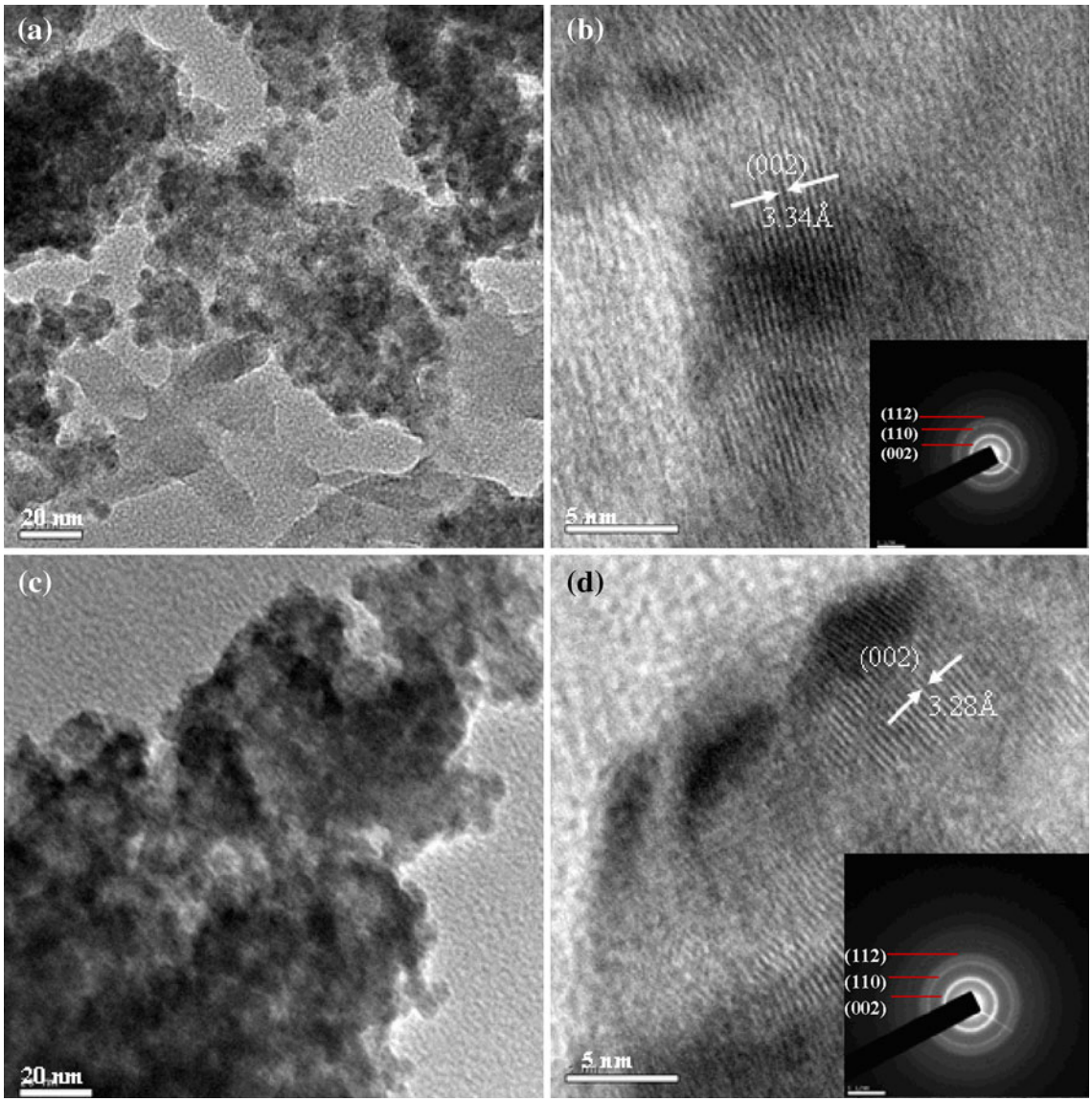

Fig. 4. HRTEM image of (a, b) CdS and (c, d) 5.02% Co-doped CdS nanoparticles.

concentration in CdS decreases the optical band gap. This decrease of energy band gap with increasing cobalt concentration is interpreted as mainly due to sp–d exchange interaction between the band electrons and the localized d electrons of the Co^{2+} ions substituting for host ions.[17] The band gap of CdS and Co-doped CdS nanoparticles are higher than that of bulk CdS (2.42 eV), and this blue-shift of the band gap occurs because of the quantum confinement effect. Semiconductor nanocrystals with particle size smaller than the Bohr radius of excitons exhibit a dominant quantum confinement effect in which size-dependent standing wave diffraction of electrons occurs as the electron moves through the interior, sensing the periodic lattice potential and the crystallite boundaries. The increase in the band gap of nanoparticles due to quantum confinement is of the quantitative form[18]

$$E_g^{nano} = E_g^{bulk} + \frac{\hbar^2\pi^2}{2\mu R^2} - \frac{1.8e^2}{\varepsilon R}, \quad (3)$$

where E_g^{nano} and E_g^{bulk} are the band gap values of the nanoparticles and the bulk material, respectively, $\mu = m_e m_h/(m_e + m_h)$ is the reduced mass, and m_e and m_h are the effective masses of electrons ($0.21m$ for CdS) in the conduction band and holes ($0.80m$ for CdS) in the valance band, respectively. e is the electron charge, ε is the relative permittivity of the semiconductor, R is the radius of the particle, and the second term is the Coulombic term and is neglected. The particle size was calculated using Eq. 3. The particle size of CdS and Co-doped CdS was found to lie in the range of 2 nm to 3 nm.

The electrical properties of materials can be studied using AC impedance data. Figure 8 shows Cole–Cole impedance plots for CdS and Co-doped

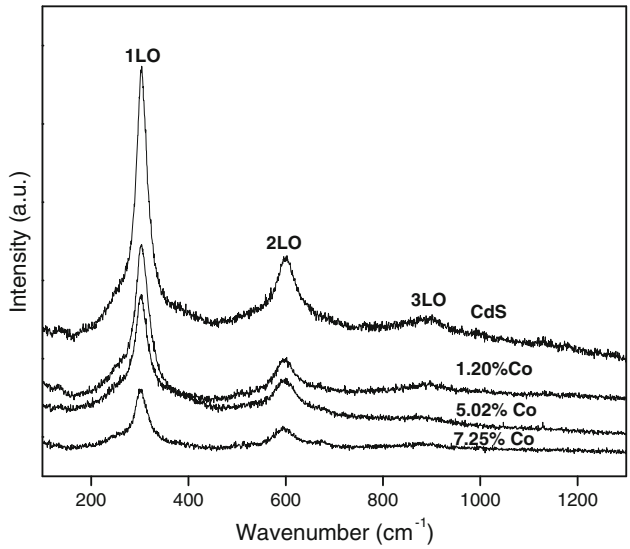

Fig. 5. Raman spectra of CdS and Co-doped CdS nanoparticles.

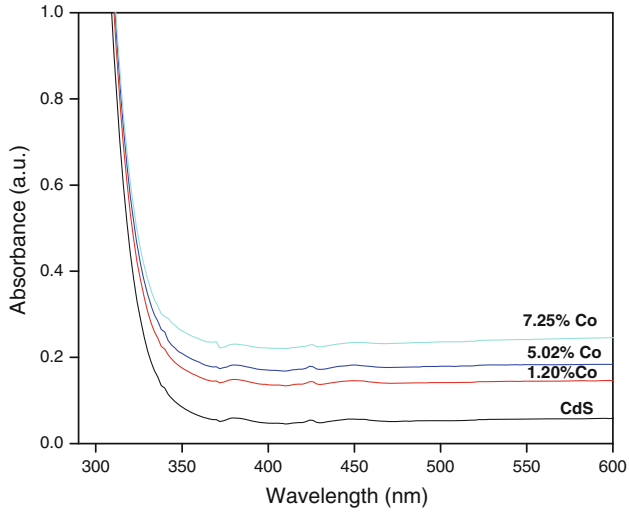

Fig. 6. Optical absorption spectra of CdS and Co-doped CdS nanoparticles.

CdS nanoparticles at different temperatures. The plots clearly show an inclined straight line in the low-frequency region, followed by a semicircular arc in the high-frequency region. The values of Z' and Z'' plotted on the complex plane take the form of semicircles, known as Cole–Cole plots.[19] It is observed from Fig. 8a that the impedance decreases with increase in temperature. Figure 8b, c clearly indicates that the impedance decreases with the increase of cobalt concentration up to 5.02%, while for further increase in cobalt concentration the impedance value is found to increase.

The bulk resistance (R_b) of the samples at various temperatures was calculated from the low-frequency intercept with the real axis using EQ software developed by Boukamp[20] for analysis of impedance data. The electrical conductivity was calculated using the equation

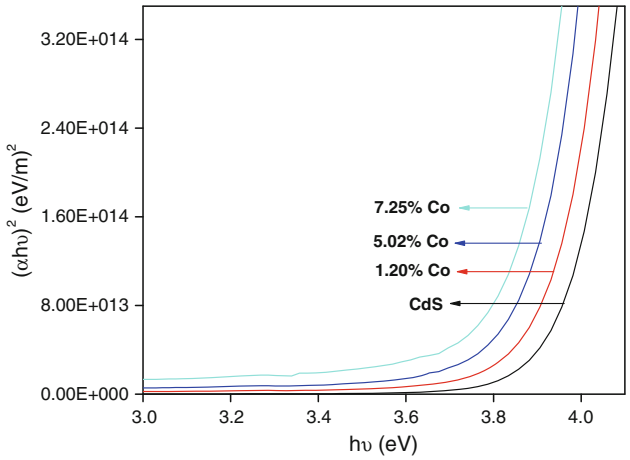

Fig. 7. $(\alpha h\upsilon)^2$ versus $h\upsilon$ plot of CdS and Co-doped CdS nanoparticles.

$$\sigma = \frac{t}{AR_b}, \tag{4}$$

where t and A are the thickness and cross-sectional area, and R_b is the bulk resistance. The conductivity values of CdS and Co-doped CdS nanoparticles were calculated, and the variation of conductivity with temperature is shown in Fig. 9. The conductivity is found to increase with increasing temperature, and the conduction mechanism in CdS and Co-doped CdS may be due to a thermally activated process. With increasing temperature, more charge carriers overcome the activation energy barrier to participate in electrical conduction. The conductivity is found to increase with Co doping concentration up to 5.02%, while beyond this concentration the conductivity is found to decrease with further increase in Co doping concentration. The increase in conductivity with increasing cobalt concentration can be related to the increase in the number of mobile charge carriers in the nanoparticles. The decrease in conductivity at higher cobalt concentration may be due to aggregation of ions, leading to formation of ion clusters. The Arrhenius plot of CdS and Co-doped CdS nanoparticles is shown in Fig. 9. The conductivity of all the samples is found to exhibit a linear variation with temperature. The temperature-dependent conductivity of all the samples obeys the Arrhenius law

$$\sigma = \sigma_0 \exp\left(\frac{-E_a}{KT}\right), \tag{5}$$

where σ_0 is the pre-exponential factor, E_a is the activation energy for conduction, T is the absolute temperature, and K is the Boltzmann constant. The activation energy of CdS was determined using Eq. 5. The activation energy of undoped CdS was obtained as 0.12 meV, while the activation energy of 1.20% Co-, 5.02% Co-, and 7.25% Co-doped CdS was found to be 0.25 meV, 0.15 meV, and 0.24 meV, respectively.

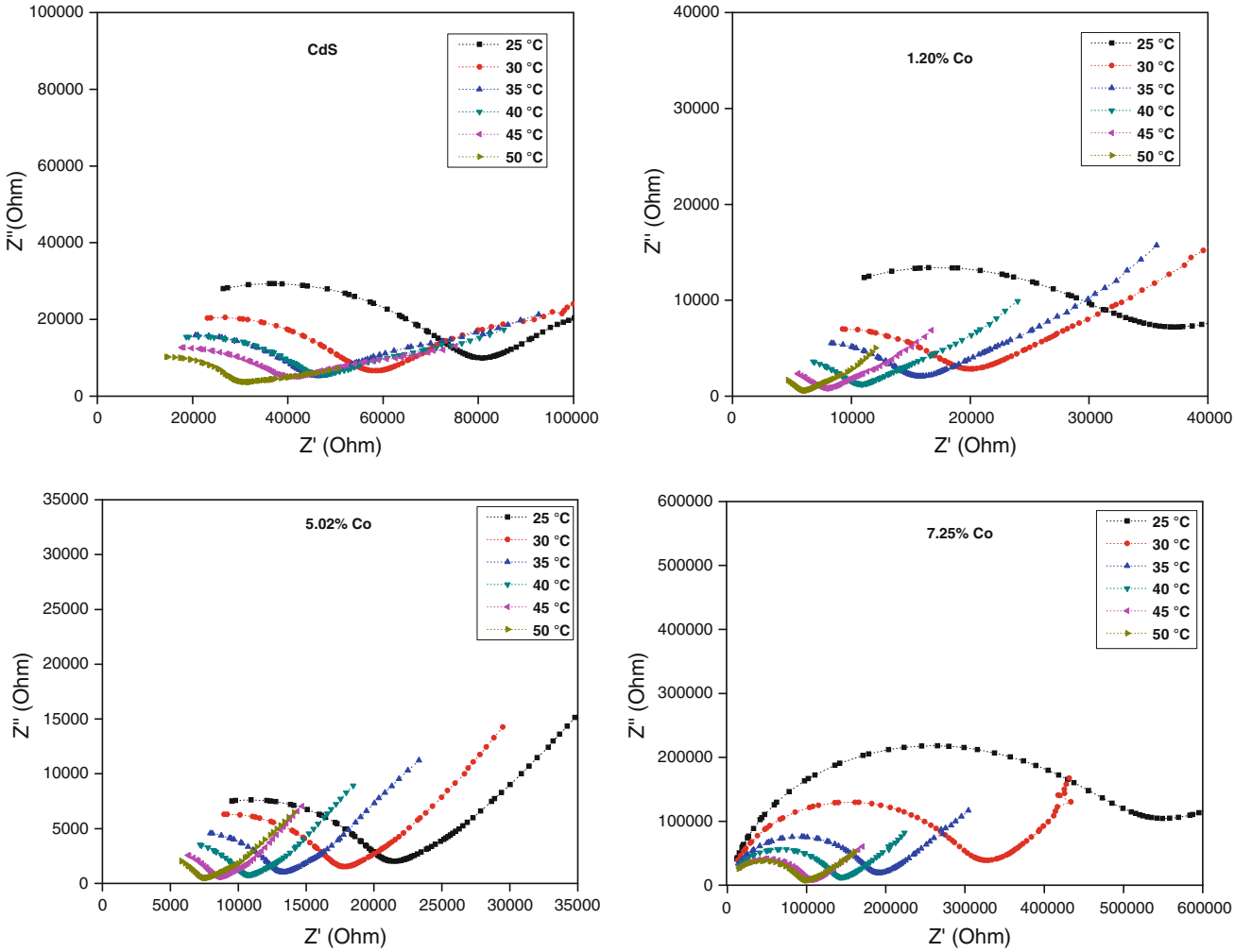

Fig. 8. Cole–Cole plot of CdS and Co-doped CdS nanoparticles for different temperatures.

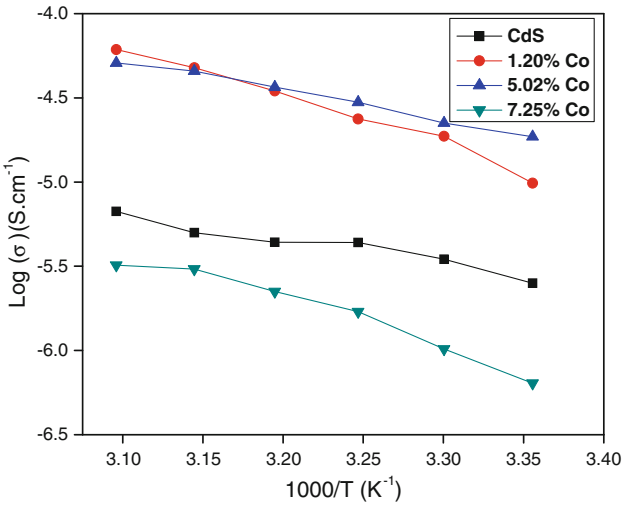

Fig. 9. Arrhenius plot of CdS and Co-doped CdS nanoparticles.

CONCLUSIONS

CdS and Co-doped CdS quantum dots were prepared by a chemical precipitation technique. X-ray diffraction results revealed that both CdS and Co-doped CdS nanoparticles exhibit hexagonal structure and that the particle size of Co-doped CdS nanoparticles is slightly greater than that of CdS. HRTEM images show the formation of CdS and Co-doped CdS quantum dots with average particle size of 2 nm to 3 nm. Optical absorption spectra of CdS and Co-doped CdS nanoparticles exhibit a blue-shift compared with bulk CdS due to the quantum confinement effect. The electrical conductivity of the CdS and Co-doped CdS nanoparticles increases with increasing temperature.

REFERENCES

1. N. Romeo, A. Bosio, and A. Romeo, *Sol. Energy Mater. Sol. Cells* 94, 2 (2010).

2. A.H. Zyoud, N. Zaatar, I. Saadeddin, C. Ali, D. Park, G. Campet, and H.S. Hilal, *J. Hazard. Mater.* 173, 318 (2010).
3. W. Lee, S.K. Min, V. Dhas, S.B. Ogale, and S.-H. Han, *Electrochem. Commun.* 11, 103 (2009).
4. J. Fan, T. Gao, G. Meng, Y. Wang, X. Liu, and L. Zhang, *Mater. Lett.* 57, 656 (2002).
5. L. Xu, Y. Su, D. Cai, Y. Chen, and Y. Feng, *Mater. Lett.* 60, 1420 (2006).
6. Y.-T. Chen, J.-B. Ding, Y. Guo, L.-B. Kong, and H.-L. Li, *Mater. Chem. Phys.* 77, 734 (2002).
7. M. Bruchez Jr, M. Moronne, P. Gin, S. Weiss, and A.P. Alivisator, *Science* 281, 2013 (1998).
8. R.S. Yadav, P. Mishra, R. Mishra, M. Kumar, and A.C. Pandey, *Ultrason. Sonochem.* 17, 116 (2010).
9. S. Arora and S. Sundar Manoharan, *Solid State Commun.* 144, 319 (2007).
10. N. Badera, B. Godbole, S.B. Srivastava, P.N. Vishwakarma, L.S. Sharath Chandra, D. Jain, M. Gangrade, T. Shripathi, V.G. Sathe, and V. Ganesan, *Appl. Surf. Sci.* 254, 7042 (2008).
11. M. Zielinski, C. Rigaux, A. Lemaitrie, and A. Mycielskin, *Phys. Rev. B* 53, 674 (1996).
12. M.J. Seong, H. Alawadhi, I. Miotkowski, and A.K. Ramdas, *Phys. Rev. B* 63, 125208 (2001).
13. N. Dixit, H. Soni, M. Chawda, and D. Bodas, *Mater. Lett.* 63, 2669 (2009).
14. J.R.L. Fernandez, M. De Souza-Parise, and P.C. Morais, *Surf. Sci.* 601, 3805 (2007).
15. M. Thambidurai, N. Muthukumarasamy, S. Agilan, N. Murugan, S. Vasantha, R. Balasundaraprabhu, and T.S. Senthil, *J. Mater. Sci.* 45, 3254 (2010).
16. S. Chandramohan, A. Kanjilal, S.N. Sarangi, S. Majumder, R. Sathyamoorthy, and T. Som, *J. Appl. Phys.* 106, 063506 (2009).
17. P. Koidl, *Phys. Rev. B* 15, 2493 (1977).
18. R. Reisfeld, *J. Alloys Compd.* 341, 56 (2002).
19. A. Laha and S.B. Krupanidhi, *Mater. Sci. Eng.* 98, 204 (2003).
20. B.A. Boukamp, *Solid State Ion.* 18–19, 136 (1986).